Stochastic Environmental Research and Risk Assessment (2018) 32:2871–2887
https://doi.org/10.1007/s00477-018-1603-4

ORIGINAL PAPER

Response of the flood peak to the spatial distribution of rainfall in the Yom River basin, Thailand

Pawee Klongvessa[1,2] · Minjiao Lu[1] · Srilert Chotpantarat[3,4,5]

Published online: 29 August 2018

Abstract

The response of the flood peak to the spatial distribution of rainfall has been reported in basins with nonuniform characteristics. However, prioritization of the influences of these characteristics is still poorly understood. This study evaluated the variability in the flood peak with the spatial distribution of rainfall at Sukhothai (city) in the Yom River basin, Thailand, and investigated the influence of the basin characteristics on the flood peak. For each of the 2-, 5- and 10-y rainfalls with durations of 24, 48 and 72 h, 1000 simulated rainfall events with various spatial distributions were generated according to the observed data by using a Monte Carlo analysis and Cholesky randomization. The floods from these rainfalls were then simulated, and the peak discharges were evaluated. The flood peaks from 24-h rainfalls were usually small but highly variable and could be extremely large when the rainfalls were concentrated over the mountainous region. The flood peaks from 48 to 72-h rainfalls were consistently large and correlated with the rainfalls over the joint area between the mountainous region and plain area. The basin characteristics that influenced the response of the flood peak to the spatial distribution of the rainfall appeared to depend on the rainfall duration and magnitude. For short-duration rainfalls, the response was mainly influenced by the surface storage when the rainfall was small and by the terrain steepness when the rainfall was large. For long-duration rainfalls, the response was mainly influenced by the soil percolation rate.

Keywords Cholesky randomization · Flood peak · Monte Carlo analysis · Rainfall spatial distribution · Yom River basin

1 Introduction

The effect of the spatial distribution of rainfall on basin discharge has been reviewed by Singh (1997), who suggested that the spatial distribution of rainfall affected the runoff timing rather than the peak discharge. Nevertheless, some studies have found that the spatial distribution of rainfall could affect the flood peak if (i) the rainfall duration was shorter than the time to equilibrium (Ogden and Julien 1993) and (ii) the basin characteristics were nonuniform (Freeze 1980; Singh 1997). Recent studies have simulated discharges from spatially distributed rainfalls over nonuniform basins and found that uniform and spatially distributed rainfall could lead to different rainfall thresholds (Golian et al. 2010, 2011), flood sources (Lee et al. 2009; Saghafian et al. 2013) and flood peaks (Chotpantarat and Chanyotha 2003; Saghafian et al. 2014; Tramblay et al. 2011; Zoccatelli et al. 2011). The basin characteristics that affected the flood peak mentioned in these studies were the hydraulic conductivity, which

✉ Pawee Klongvessa
nineboon@hotmail.com

1 Department of Civil and Environmental Engineering, Graduate School of Engineering, Nagaoka University of Technology, Kamitomioka 1603-1, Nagaoka, Niigata 940-2188, Japan

2 Department of Environmental Technology and Management, Faculty of Environment, Kasetsart University, 50 Ngam Wong Wan Road, Chatuchak, Bangkok 10900, Thailand

3 Department of Geology, Faculty of Science, Chulalongkorn University, 254 Phyathai Road, Pathumwan, Bangkok 10330, Thailand

4 Research Program in Control of Hazardous Contaminants in Raw Water Resources for Water Scarcity Resilience, Center of Excellence on Hazardous Substance Management (HSM), Chulalongkorn University, 254 Phyathai Road, Pathumwan, Bangkok 10330, Thailand

5 Research Unit Control of Emerging Micropollutants in Environment, Chulalongkorn University, 254 Phyathai Road, Pathumwan, Bangkok 10330, Thailand

controlled the amount of excess rainfall, and topography, which controlled the attenuation. Other characteristics that could influence the flood peak were the shape, storage and roughness of the area. The spatial data have been taken into account in flood simulations in many studies (Hamidi et al. 2018; Klongvessa and Chotpantarat 2014; Meng et al. 2017; Nkiaka et al. 2018; Samadi et al. 2018).

However, prioritization of the influences of each characteristic is still poorly understood. If the influences of these characteristics were prioritized, it would be easier to determine the locations where rainfall has a strong impact on the peak discharge from these basin characteristics; moreover, it would be easier to create a numerical model that focuses on only the important characteristics. In this study, the peak discharges from various spatially distributed rainfalls were simulated, similar to the approach used in previous studies, but then the response of the peak discharge to the rainfall at each location were further investigated. Finally, the characteristics of the location where the response was most pronounced were identified, and the influence of each characteristic was then analyzed. With this approach, the influence of each characteristic was prioritized.

The Yom River basin, northern Thailand (see Sect. 2) was chosen for this study because it is large and long, leading to a longer time to equilibrium, and there are clearly different characteristics between the upstream and downstream areas of this basin. The upstream area is a forested mountainous region, while the downstream area is an agricultural plain area. Moreover, the flow in this basin is primarily natural, since there are no large-scale control structures along the river. Furthermore, the long shape of the basin drives a clear variability in the rainfall locations. For these reasons, the Yom River basin was deemed to be appropriate for studying the response of the flood peak to the spatial distribution of rainfall.

2 Study area

The Yom River basin is in northern Thailand and covers an area of approximately 24,000 km^2 (Fig. 1). The length of the main stream, the Yom River, is approximately 700 km. The basin was divided into the three parts: the upper, middle and lower Yom basin. However, the upper part was excluded from this study because there is a weir near the boundary between the upper and middle Yom basin (Fig. 1), which can affect the natural flow. Apart from this weir, there are no large-scale control structures in the basin. Several small floodgates for irrigation have been constructed but do not significantly affect the flow.

The study area of the middle and lower Yom basin covers an area of approximately 19,000 km^2, and the

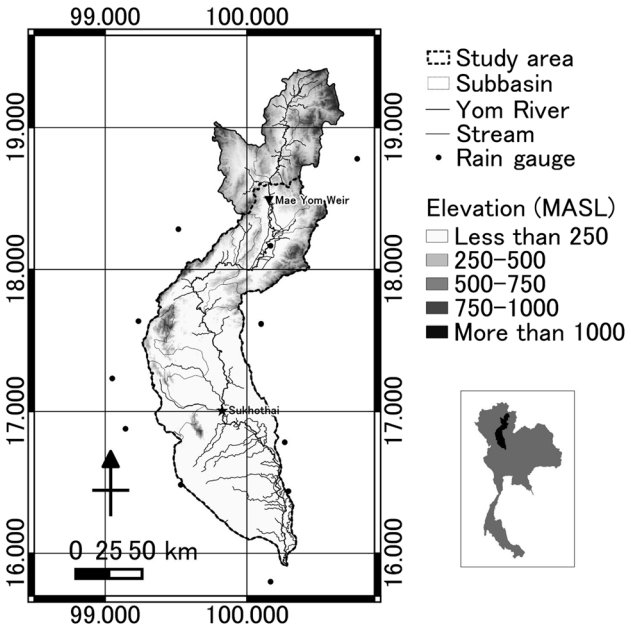

Fig. 1 Location of the study area (Yom River basin, Northern Thailand)

length of the main stream was approximately 600 km. The downstream part of the area is a plain that is mostly agricultural with some surface water storage. The soil in this part of the study area is mainly a fine-textured soil. The upstream part of the study area is a mountainous region and mostly covered by forest with a coarser soil texture than that downstream. Most of the flood simulations over the Yom River basin and the Chao Praya basin, in which the Yom River basin is located, have used two-dimensional models (Hunukumbura and Tachikawa 2012; Kotsuki and Tanaka 2013; Sayama et al. 2015, 2017; Sriariyawat et al. 2013) or a one-dimensional model at a sub-basin scale (Klongvessa et al. 2017b; Kure and Tebakari 2012; Tingsanchali and Karim 2010), where nonuniform rainfall or basin characteristics can be considered.

Rainfall in the study area is high during May–October, but floods mostly occur during September–October when the rainwater from rainfalls during the previous months saturates the soil and decreases the rainwater storage capacity for subsequent rainfalls (Chotpantarat and Boonkaewwan 2018; Kotsuki and Tanaka 2013). The city of Sukhothai, which is located within the study area (Fig. 1), is frequently damaged by floods due to the low retention capability of the upstream area and the narrow basin cross section in the downstream area (Sriariyawat et al. 2013).

3 Methodology

3.1 Model description

This study used the HEC-HMS model (Feldman 2000) to simulate rainfall runoff. However, due to the long main river, the river flow could play an important role on traveling of water. Therefore, the runoff simply predicted by the transformation from excess rainwater in the HEC-HMS model might not be very accurate. We improved the accuracy by using the physically-based HEC-RAS model (Brunner 2010) to simulate the river flow. The runoff simulated by the HEC-HMS model determined the lateral flow to the river, and the river flow was routed by the HEC-RAS model. The timestep for the simulation was 15 min and the distance between calculation points along the river was set to be closet to but not more than 5 km.

In the HEC-HMS model, the excess rainwater was controlled by a constant percolation loss and surface water storage volume. In this study, the infiltration storage was assumed to be full because flooding in the study area is mostly associated with a saturated soil condition (Kotsuki and Tanaka 2013). The excess rainwater was transformed to runoff by Snyder's unit hydrograph method, which is characterized by the standard lag time and peak coefficient. The standard lag time varied upon the shape and characteristics of the drainage area, as shown in Eq. (1) (Feldman 2000);

$$t_p = 0.75 C_t (L L_c)^{0.3}, \quad (1)$$

where t_p is the standard lag time (h); C_t is the non-physically based basin coefficient, which is generally affected by topography and was low over the mountainous region; L is the distance from an outlet to the farthest boundary (km); and L_c is the centroid distance (km). The peak coefficient is a non-physical parameter that determines the peak height, and is generally high when C_t is low.

In the HEC-RAS model, the flow was routed along the river by the principles of conservation of mass and conservation of momentum using a four-point implicit scheme (Brunner 2010). The river was characterized by Manning's roughness coefficient (n).

The conceptual model of the study area was developed in Klongvessa et al. (2017b). The study area was divided into 13 subareas, in which the rainfall was transformed into lateral flow to the main stream (Fig. 2 and Table 1). The upper four subareas represent the mountainous region and were calibrated separately from the lower nine subareas that represent the plain. However, in the experimental simulation, since the water level in the city of Sukhothai (stream gauge Y4) did not respond to the rainfall in the five downstream subareas, the rainfall could be simulated over only the other eight subareas. The rainfall was spatially distributed across four zones (Fig. 2 and Table 1), following the methods of Klongvessa et al. (2017b), who had shown that distributing the rainfall across these four zones could still drive accurate simulation results that were similar to the simulation results when the rainfall was distributed across eight subareas. These four zones are referred to as zones 1–4, according to their locations: the most upstream zone was zone 1 and the most downstream zone was zone 4. Zones 1 and 2 represent the mountainous region, while zones 3 and 4 represent the plain area. The result of the model validation is shown in Fig. 3. It can be seen that the model could simulate the traveling of flood peak accurately with root-mean-square errors (RMSE) of at most approximately 1.0 m for the recent years (2012–2014). For the year 2011, the RMSE's were large because the river cross sections were changed by the big flood.

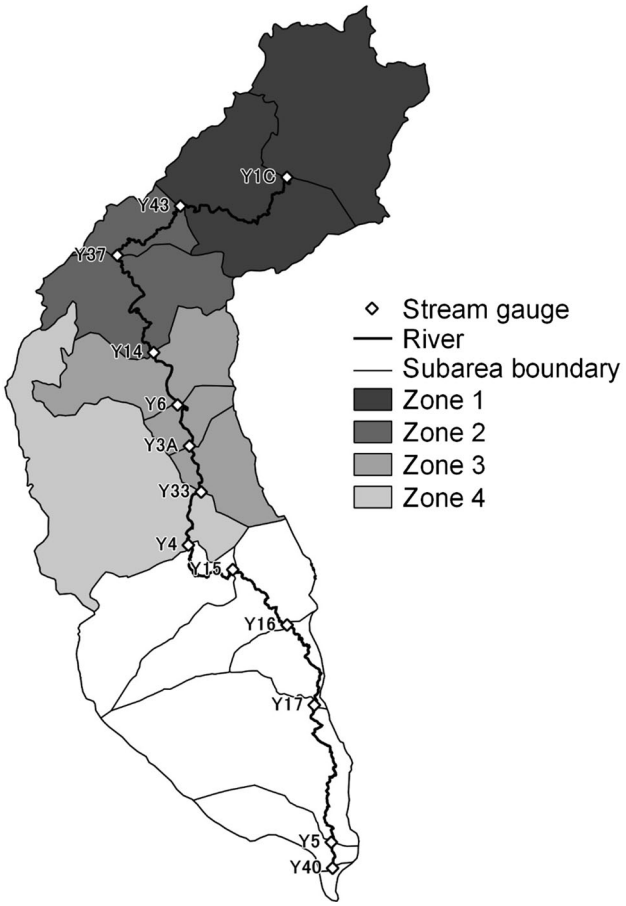

Fig. 2 Digitized study area for the simulations, showing also the location of the 13 outlet stream gauges (Y1–Y43)

The calibrated parameters are shown in Table 2. Zones 1 and 2 were characterized by a high percolation rate due to the coarser soil texture observed in these zones than in zones 3 and 4, a high channel Manning's n due to the

Table 1 Details of the 13 subareas within the study area

Outlet stream gauge	Upstream distance (km)	Zone	Area (km^2)	L_c (km)	L (km)	Slope[a] (%)
Y1C	490.5	1	2457.0	27.9	63.7	15
Y43	433.9	1	2075.6	22.6	57.3	14
Y37	384.5	2	544.1	12.2	27.2	16
Y14	322.7	2	1544.9	20.6	43.8	14
Y6	297.5	3	1364.1	16.2	48.0	12
Y3A	275.8	3	370.3	9.6	24.9	1
Y33	251.9	3	702.1	10.7	31.1	1
Y4	219.0	4	3410.7	35.2	106.9	8
Y15	175.0	–	1465.3	32.9	66.7	4
Y16	129.4	–	1505.8	17.8	64.5	0
Y17	84.4	–	528.1	17.7	32.7	0
Y5	13.5	–	2637.2	43.9	88.3	0
Y40	0.0	–	632.5	24.7	51.4	0

[a]The slope was calculated from the 90 m digital elevation map generated from the 1:50,000 topographic map from the Royal Thai Survey Department

vegetation over the forestland (Chow et al. 1988), a low basin coefficient [C_t in Eq. (1)] due to the steepness (Feldman 2000) and a low surface water storage. The relative magnitude of the values of these four parameters were reversed for zones 3 and 4, which had a different soil texture, land use and steepness than those of zones 1 and 2.

3.2 Rainfall design

The total rainfall amount and temporal distribution used in this study were from Klongvessa et al. (2017b). That study determined the amounts of 2-, 5- and 10-y rainfalls under durations of 24, 48 and 72 h and designed the hyetograph from the data during May–October 1981–2010 collected every 3 h at 11 high quality rain gauges operated by Thai Meteorological Department (TMD). The locations of these rain gauges are shown in the Fig. 1. Even though most of the rain gauges were located outside the Yom River basin, the rainfall amounts collected at these rain gauges have been found to be consistent with rainfall amounts collected at 24 local rain gauges inside the basin (Chotpantarat et al. 2013). Therefore, they were capable of representing the rainfall in our study area. Because the rainfall amounts at the local rain gauges were collected on a daily basis, not every 3 h, they could not be used for the rainfall design in the study. Hence, only the rainfall data at the rain gauges shown in the Fig. 1 were used. The amounts of 2-, 5- and 10-y rainfalls were determined using the Weibull equation (Singh 1992) and generalized extreme value (GEV) distribution (Martins and Stedinger 2000), while the rainfall temporal distribution was determined from the observed areal rainfalls over each of the zones 1–4 with the timestep of 3 h by the alternating block method (Chow et al. 1988). Mostly, the duration of these observed rainfalls ranged from a few hours to 3 days. These calculations were shown to accurately represent the rainfall in the study area. The rainfall amount at each return period and duration is shown in Table 3.

A total of 1000 spatial distributions of rainfall were created according to the observed data and simulated using a Monte Carlo analysis (Golian et al. 2010, 2011) and Cholesky randomization approach (Kreyszig 1999). First, observed rainfall events were selected; in this study, the spatial distribution characteristics of the 24-, 48- and 72-h rainfalls were distinguished. The 24-h rainfall was determined from observed events that had days with rainfall greater than 35.0 mm, while the 48-h and 72-h rainfalls were determined from the observed events that had 2 and 3 consecutive days rainfall greater than 35.0 mm, respectively. The rainfall data were observed at the 11 rain gauges during May–October 1981–2010 (Fig. 1), and the zonal rainfalls were calculated from the Thiessen weighted average for the zones 1-4. A total of 728, 249 and 104 events were used to determine the characteristics of the 24-, 48- and 72-h rainfalls, respectively. The criterion of greater than 35.0 mm/day rainfall was used because it is the same criterion that the TMD used to classify heavy rainfall days. Then, for each of the selected events, the rainfall was converted to dimensionless rainfall by dividing the zonal rainfall amount (rainfall amount in each of the four zones) with the average areal rainfall amount. Next, the probability distribution of the dimensionless rainfall in each zone (Sect. 3.2.1) and the spatial correlations of the dimensionless rainfall among the zones were determined. Subsequently, the dimensionless rainfall in each of the four zones was randomized according to the determined probability distributions and spatial correlations (Sect. 3.2.2). Finally, the dimensionless random rainfall distributions

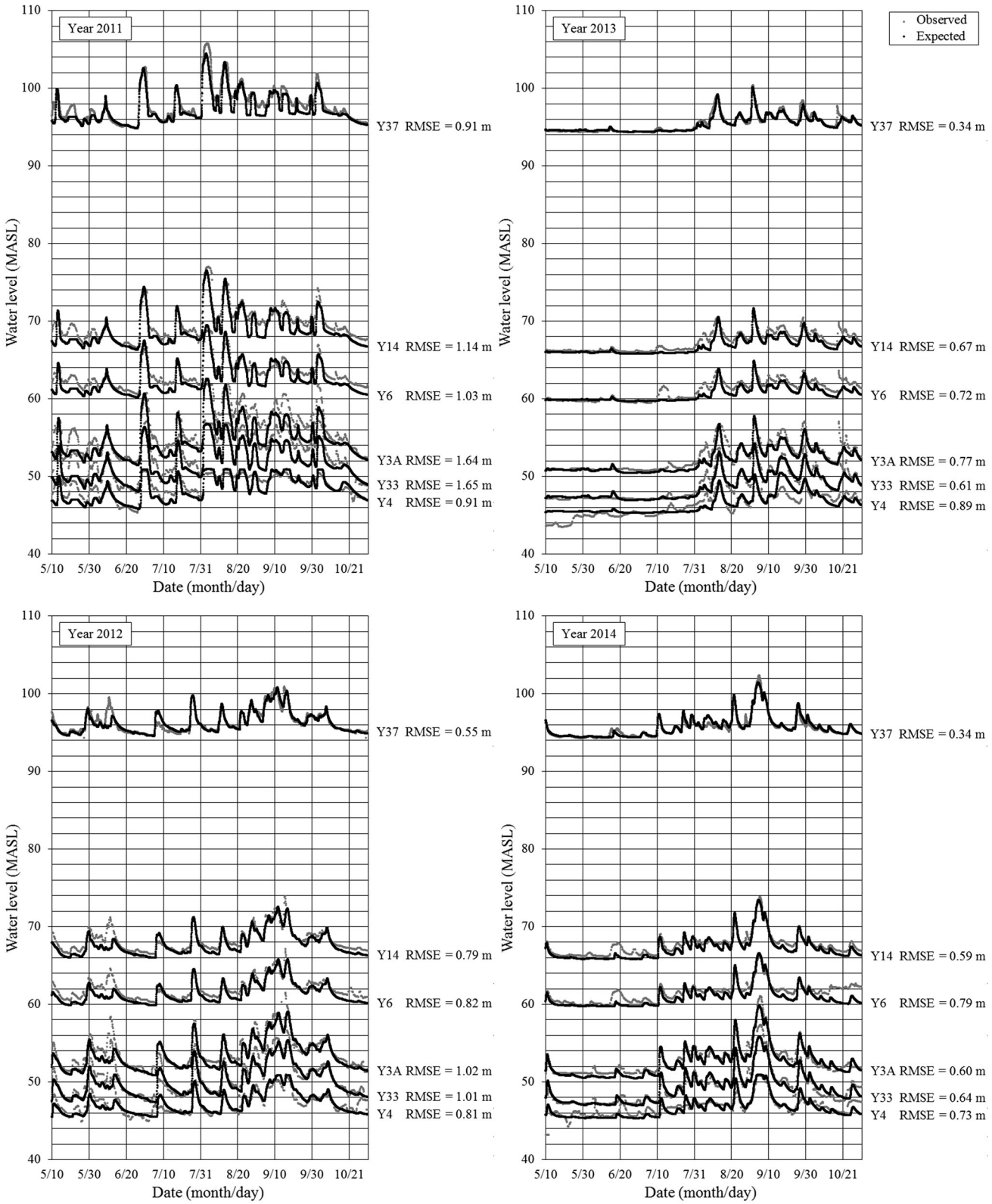

The stream gauge Y43 was not used for the validation because the quality of the data at that stream gauge was not very good.

RMSE's shown in the table may be slightly different from those shown in Klongvessa et al. (2017b) because they validated the result before grouping the subareas into 4 zones while this study validated after the grouping.

Fig. 3 Result of model validation at the stream gauges along the Yom River (Y37, Y14, Y6, Y3A, Y33 and Y4) and root-mean-square error (RMSE) between observed and expected water levels

Table 2 Model parameters (Klongvessa et al. 2017b)

Parameter	Zones 1–2	Zones 3–4
Percolation rate	2.95 mm/h	0.45 mm/h
Surface storage	0 mm	30 mm
Basin constant (C_t)	2.9	5.8
Peak coefficient (C_p)	0.16	0.18
Channel Manning's n	0.047	0.019

were converted to the dimensional rainfall by multiplying the dimensionless amounts with the determined amount (Table 3).

3.2.1 Probability distribution of the zonal dimensionless rainfall

In the Monte Carlo analysis, the probability distribution of the zonal dimensionless rainfall was determined by fitting the probability of the observed zonal dimensionless rainfall amount with a statistical distribution before generating the random rainfalls according to the same statistical distribution (Golian et al. 2010, 2011). First, the Weibull equation (Singh 1992) was applied to assign the probabilities to the observed data. Next, the normal distribution was used to fit the observed data using Eq. (2);

$$x = \begin{cases} \mu + \sigma\sqrt{2}erf^{-1}(1-2P), \mu + \sigma\sqrt{2}erf^{-1}(1-2P) \geq 0 \\ 0, \mu + \sigma\sqrt{2}erf^{-1}(1-2P) < 0 \end{cases}, \quad (2)$$

where x is the expected zonal dimensionless rainfall amount, μ is a location parameter, σ is a scale parameter, erf is an error function and P is the exceedance probability.

It should be noted that the rainfall amount cannot be negative; therefore, the dimensionless rainfall amount should be set to 0 if the expected amount determined by the normal distribution was negative.

3.2.2 Rainfall randomization

The zonal dimensionless rainfalls were randomized according to (i) the location parameter (μ) and scale parameter (σ) of the normal distribution, which was used to fit the observed data with Eq. (2), and (ii) the spatial correlations of the data in zones 1–4. This process was performed with four series of normally distributed random numbers (which represent the rainfall in the four zones); the series have specified correlation coefficients. These series of random numbers were generated by Cholesky randomization (Kreyszig 1999).

Let $\boldsymbol{V}_1 = [v_{1,1} \quad v_{2,1} \quad \ldots \quad v_{1000,1}]$, $\boldsymbol{V}_2 = [v_{1,2} \quad v_{2,2} \quad \ldots v_{1000,2}]$, $\boldsymbol{V}_3 = [v_{1,3} \quad v_{2,3} \quad \ldots \quad v_{1000,3}]$ and $\boldsymbol{V}_4 = [v_{1,4} \quad v_{2,4} \quad \ldots \quad v_{1000,4}]$ be vectors of independent

Table 3 Amount of the 2-, 5- and 10-y rainfalls with 24-, 48- and 72-h durations (Klongvessa et al. 2017b)

Return period	24-h duration (mm)	48-h duration (mm)	72-h duration (mm)
2 y	57.4	79.7	99.9
5 y	78.0	106.9	136.1
10 y	92.6	123.1	155.8

Table 4 Parameters of the normal distribution used to fit the zonal dimensionless rainfall, RMSE between the observed and expected values, and test and critical values of the Chi square goodness of fit test

Duration	Zone	μ	σ	RMSE	Test value	Critical value[a]
24 h	1	0.68299	0.84794	0.0869	36.02	628.75
	2	0.93682	0.86307	0.2235	42.88	683.22
	3	1.05122	0.73598	0.0642	18.93	731.33
	4	1.09418	1.07667	0.1774	216.53	671.71
48 h	1	0.84184	0.52160	0.0630	5.20	269.61
	2	1.04170	0.44978	0.1054	2.29	281.44
	3	1.15603	0.50492	0.0514	1.94	281.44
	4	1.02929	0.64447	0.1473	33.04	269.61
72 h	1	0.82995	0.40852	0.0341	0.33	123.23
	2	1.05375	0.36577	0.0791	0.44	125.46
	3	1.15477	0.42262	0.0550	0.48	125.46
	4	1.06650	0.58129	0.1486	6.70	122.11

[a]Critical value is at a significance level of 0.05

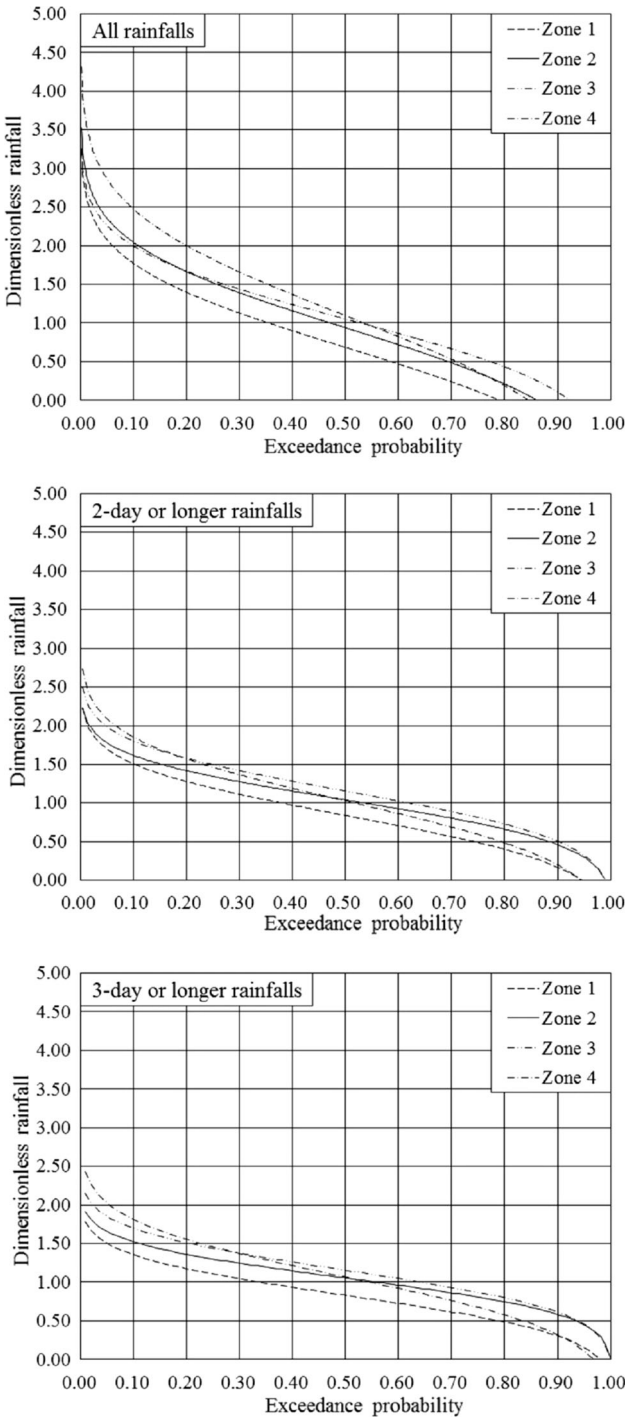

Fig. 4 Zonal dimensionless rainfall probabilities calculated from all rainfalls, 2-day or longer rainfalls and 3-day or longer rainfalls

random numbers with a standard normal distribution, and let $c_{i,j}$ be a correlation coefficient between the dimensionless rainfalls in zones i and j. The matrix of random numbers $\boldsymbol{V}$ and matrix of correlations $\boldsymbol{C}$ can be written as Eqs. (3) and (4), respectively;

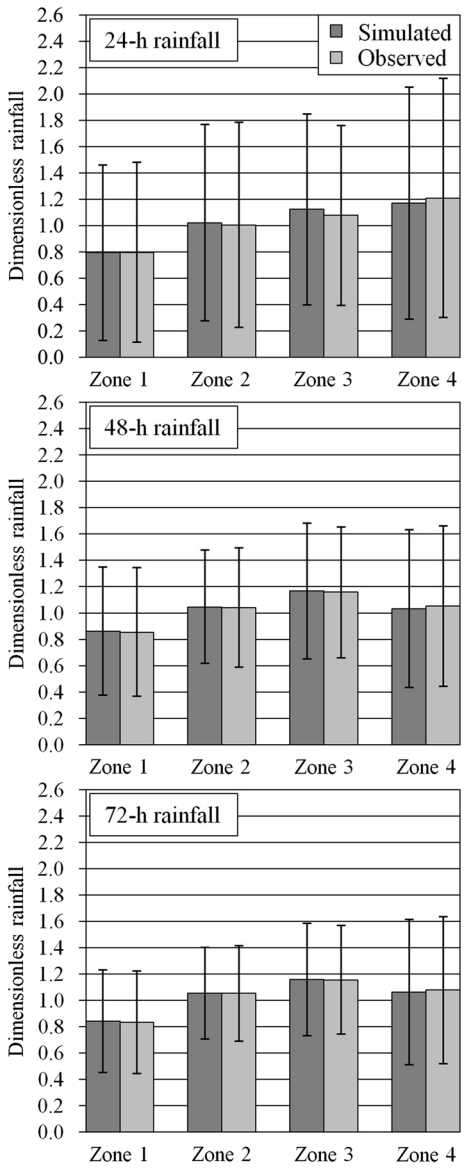

Fig. 5 Averages and standard deviations (whiskers) of simulated and observed zonal dimensionless rainfalls

$$\boldsymbol{V} = \begin{bmatrix} v_{1,1} & v_{1,2} & v_{1,3} & v_{1,4} \\ v_{2,1} & v_{2,2} & v_{2,3} & v_{2,4} \\ \vdots & \vdots & \vdots & \vdots \\ v_{1000,1} & v_{1000,2} & v_{1000,3} & v_{1000,4} \end{bmatrix}, \tag{3}$$

$$\boldsymbol{C} = \begin{bmatrix} 1 & c_{1,2} & c_{1,3} & c_{1,4} \\ c_{1,2} & 1 & c_{2,3} & c_{2,4} \\ c_{1,3} & c_{2,3} & 1 & c_{3,4} \\ c_{1,4} & c_{2,4} & c_{3,4} & 1 \end{bmatrix}. \tag{4}$$

The Cholesky component $\boldsymbol{Z}$ of the matrix $\boldsymbol{C}$ is defined as the triangular matrix that satisfied Eq. (5);

$$\boldsymbol{C} = \boldsymbol{Z}\boldsymbol{Z}^{\mathrm{T}}. \tag{5}$$

The matrix V^{*} is defined by Eq. (6);

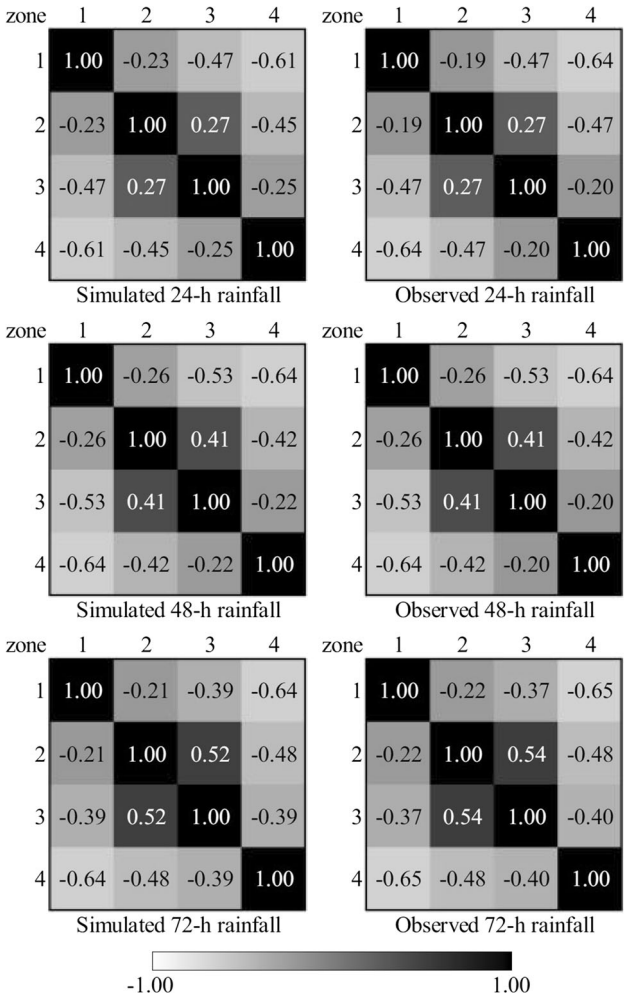

Fig. 6 Spatial correlation of the simulated and observed zonal dimensionless rainfalls

$$\boldsymbol{V}^* = \boldsymbol{V}\boldsymbol{Z} = \begin{bmatrix} v^*_{1,1} & v^*_{1,2} & v^*_{1,3} & v^*_{1,4} \\ v^*_{2,1} & v^*_{2,2} & v^*_{2,3} & v^*_{2,4} \\ \vdots & \vdots & \vdots & \vdots \\ v^*_{1000,1} & v^*_{1000,2} & v^*_{1000,3} & v^*_{1000,4} \end{bmatrix}. \quad (6)$$

The correlation between the components of vectors $\boldsymbol{V}^*_{\boldsymbol{i}} = \begin{bmatrix} v^*_{1,i} & v^*_{2,i} & \cdots & v^*_{1000,i} \end{bmatrix}$ and $\boldsymbol{V}^*_{\boldsymbol{j}} = \begin{bmatrix} v^*_{1,j} & v^*_{2,j} & \cdots & v^*_{1000,j} \end{bmatrix}$ where $i, j \in \{1, 2, 3, 4\}$ is $c_{i,j}$, and these components have a standard normal distribution. Therefore, in the event $r \in \{1, 2, \ldots, 1000\}$, the dimensionless rainfall amount in the zone $c \in \{1, 2, 3, 4\}$ can be calculated from Eq. (7);

$$x = \begin{cases} \mu + \sigma v^*_{r,c}, & \mu + \sigma v^*_{r,c} \geq 0 \\ 0, & \mu + \sigma v^*_{r,c} < 0 \end{cases}, \quad (7)$$

where x is the dimensionless rainfall amount and μ and σ are also used in Eq. (2). However, for some matrix $\boldsymbol{C}$, there is no matrix $\boldsymbol{Z}$ that can satisfy Eq. (5). In these cases, some values of $c_{i,j}$ were slightly adjusted (Higham 2002).

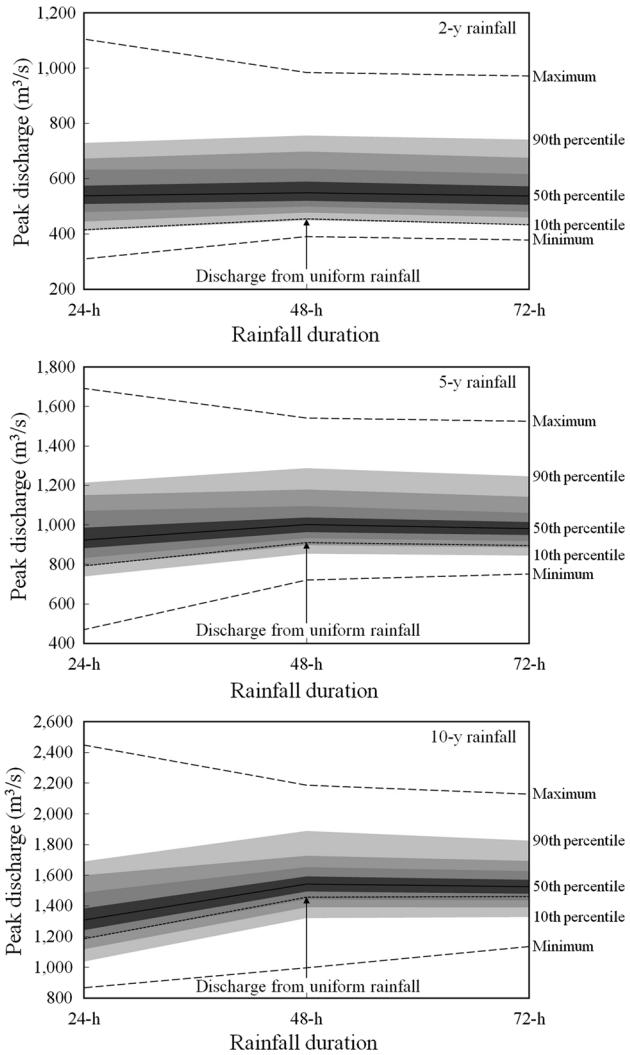

Fig. 7 Simulated peak discharges at Sukhothai city from 1000 simulated rainfalls of 2-y, 5-y and 10-y return periods and 24-, 48- and 72-h durations

It should be noted that in the observed data, the areal average of the dimensionless rainfall for each event was 1, but for random events, the areal average dimensionless rainfall might not be equal to 1 due to the randomness of the inputs. Therefore, before the conversion of the random dimensionless rainfall to dimensional rainfall by using a determined amount, the random zonal dimensionless rainfalls must be reweighted to calibrate the areal average values to 1.

4 Results and discussion

4.1 Spatial rainfall

The parameters of the normal distribution used to fit the zonal dimensionless rainfall, as in Eq. (2), are shown in

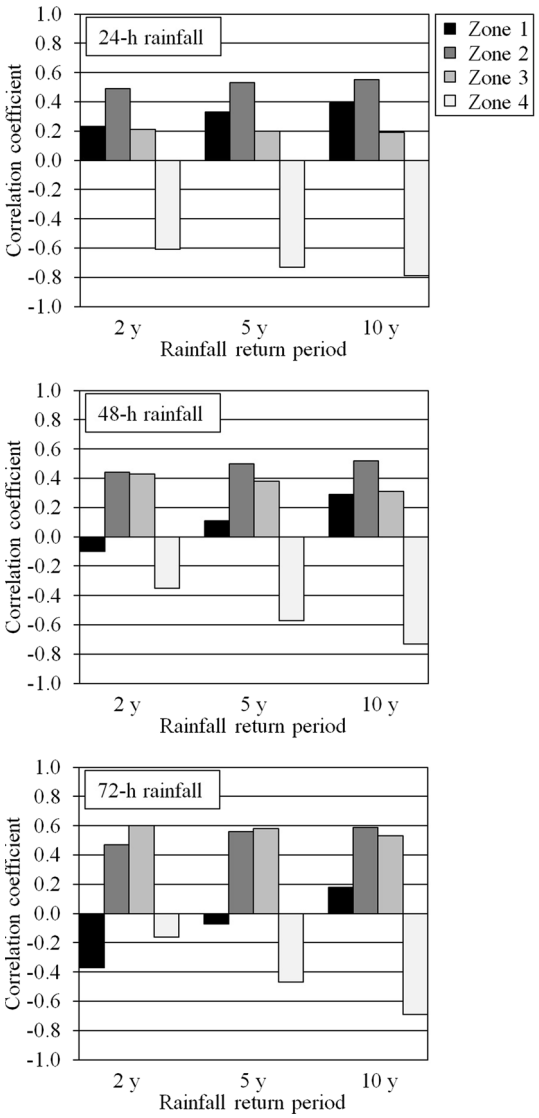

Fig. 8 Correlation coefficient between the peak discharge and peak rainfall intensity in each zone

Table 4, and the plots of the distributions are shown in Fig. 4. The Chi square goodness of fit test confirmed that Eq. (2) can fit the data at the 0.05 significance level (Table 4). Comparisons of the dimensionless rainfalls generated by the Monte Carlo analysis with Cholesky randomization and the observed dimensionless rainfalls are shown in Fig. 5, which provides the averages and standard deviations, and Fig. 6, which provides the spatial correlations; the generated and observed dimensionless rainfalls were similar. The positive correlation between rainfalls in zones 2 and 3 and the negative correlations for the other zones suggest that the rainfall location can be classified into 3 groups, zone 1, zones 2–3 and zone 4. This classification coincides with the study by Klongvessa et al. (2017a) who have divided the northern Thailand into 3 parts according to the characteristics of consecutive rainfall days, the mountainous region (zone 1 in our study) with low rainfall amount, the plain area (zone 4 in our study) with higher rainfall amount than the mountainous region and the joint area (zones 2–3 in our study) with high probability of consecutive heavy rainfall days. Unlike the short-duration (24-h) rainfall, the long-duration (48- and 72-h) rainfalls tended to be more concentrated upstream, since the 48- and 72-h rainfalls were more common than the 24-h rainfall in zones 1–3, while the 24-h rainfall were more common than the 48- and 72-h rainfalls in zone 4. However, all short- and long-duration rainfalls tended to be more concentrated over the downstream part of the study area than the upstream part.

4.2 Flood peak

Flood peaks in the city of Sukhothai from the 2-, 5- and 10-y rainfalls with 24-, 48- and 72-h durations are shown in Fig. 7. The flood peak from a 24-h rainfall was usually low but highly variable, while those from 48 to 72-h rainfalls were high and fairly uniform. From Fig. 7, it can be seen that in some rare cases, a 24-h rainfall can produce an extremely high flood peak that is even higher than the highest flood peaks from the 48- and 72-h rainfalls.

The spatial distribution of the rainfall that caused the high flood peaks was evaluated by determination of the correlation coefficient between the flood peak and peak rainfall intensity in each of the four zones (Fig. 8). The flood peak from a 24-h rainfall was high when the rainfall was concentrated over zones 1 and 2 (upstream area), while the flood peaks from the 48- and 72-h rainfalls were high when the rainfalls were concentrated over zones 2 and 3 (joint area). The negative correlation for the zone 4 suggests that the high peak discharge at the Sukhothai city is caused by discharge from the upstream rainfall rather than the local rainfall (rainfall in zone 4). Given a fixed areal rainfall amount, the higher rainfall amount in the upstream area means the lower rainfall amount in the local area. With this reason, the correlations between the peak discharges and peak rainfall intensities in the zone 4 are negative.

The flood peak from a 24-h rainfall was low because the rainfall duration was shorter than the concentration times, which was 48–72 h depending on the rainfall location (Klongvessa et al. 2017b); moreover, 24-h rainfalls were rarely concentrated over zones 1 and 2 (Fig. 5). The high variability in the flood peaks from the 24-h rainfall was because the rainfall duration was shorter than the concentration time, and the equilibrium point, where the incoming water from the rainfall is balanced with the outgoing discharge, was not reached (Ogden and Julien 1993). Conversely, the flood peaks from the 48- and 72-h rainfalls were high because the rainfall durations were similar to the

Table 5 Peak discharge (m^3/s) from one sample of 24-h rainfalls with a 2-y return period that concentrated over the mountainous region and one sample of those over the plain area when the basin coefficient, surface storage, Channel Manning's n and percolation rate were adjusted to be uniform

Adjustment detail	Concentrated over the mountains		Concentrated over the plains	
	Peak discharge	Difference[a]	Peak discharge	Difference[a]
Basin coefficient is 2.9	573.6	243.2	818.0	366.1
Basin coefficient is 5.8	330.4		451.9	
Surface storage is 0 mm	692.0	563.0	761.3	381.5
Surface storage is 30 mm	129.0		379.8	
Channel Manning's n is 0.047	510.2	83.2	502.5	35.0
Channel Manning's n is 0.019	593.4		537.5	
Percolation rate is 2.95 mm/h	453.2	520.9	291.8	422.5
Percolation rate is 0.45 mm/h	974.2		714.3	
No adjustment	541.7	–	539.3	–

[a]Difference in the peak discharges between when parameter values at the mountainous region and plain area were used

Table 6 Peak discharge (m^3/s) from one sample of 24-h rainfalls with a 10-y return period that concentrated over the mountainous region and one sample of those over the plain area, when the basin coefficient, surface storage, Channel Manning's n and percolation rate were adjusted to be uniform

Adjustment detail	Concentrated over mountains		Concentrated over plains	
	Peak discharge	Difference[a]	Peak discharge	Difference[a]
Basin coefficient is 2.9	1543.2	672.9	1971.0	896.5
Basin coefficient is 5.8	861.3		1074.5	
Surface storage is 0 mm	1617.9	640.6	1499.5	377.6
Surface storage is 30 mm	977.3		1121.9	
Channel Manning's n is 0.047	1317.2	207.2	1197.5	70.7
Channel Manning's n is 0.019	1524.4		1268.2	
Percolation rate is 2.95 mm/h	1281.5	652.0	993.5	518.0
Percolation rate is 0.45 mm/h	1933.5		1511.5	
No adjustment	1415.9	–	1278.8	–

[a]Difference in the peak discharges between when parameter values at the mountainous region and plain area were used

concentration time, and these rainfalls tended to concentrate over zones 2 and 3. The flood peaks from those rainfalls were not considerably variable because the equilibrium point had been reached.

4.3 Influence of basin characteristics

In this section, the physical mechanism behind the correlation between the flood peak and the rainfall intensity was investigated in each zone.

4.3.1 Short-duration rainfall

The flood peak from a short-duration rainfall appeared to respond to the rainfall in zones 1 and 2 more strongly than the rainfall in zones 3 and 4. The differences in the basin parameters between zones 1 and 2 and zones 3 and 4 included the percolation rates, surface water storage, basin constants [C_t in Eq. (1)], peak coefficients for the Snyder unit hydrograph transformation and channel Manning's n. These characteristics were evaluated by performing simulations with uniform parameters to determine which characteristic had the most influence on the peak discharge. For each parameter, the value over zones 1 and 2 was used for the first simulation, and the value over zones 3 and 4 was used for the second simulation; the influence of each parameter can then be determined by evaluating the difference between the simulated peak discharges from these two simulations.

The influence of each parameter appeared to depend on the rainfall amount and whether the rainfall was concentrated over the mountainous region or the plain area. Table 5 shows the results from the simulations of two samples of 2-y rainfalls with 24-h duration when each parameter was adjusted to be uniform. One sample was concentrated over the mountainous region, while another sample was concentrated over the plain area. Table 6 is similar to Table 5 but for samples of 10-y rainfalls. The rainfall hyetographs and discharges at the outlets of the zones 1–4 for the usual case (no adjustment of parameter)

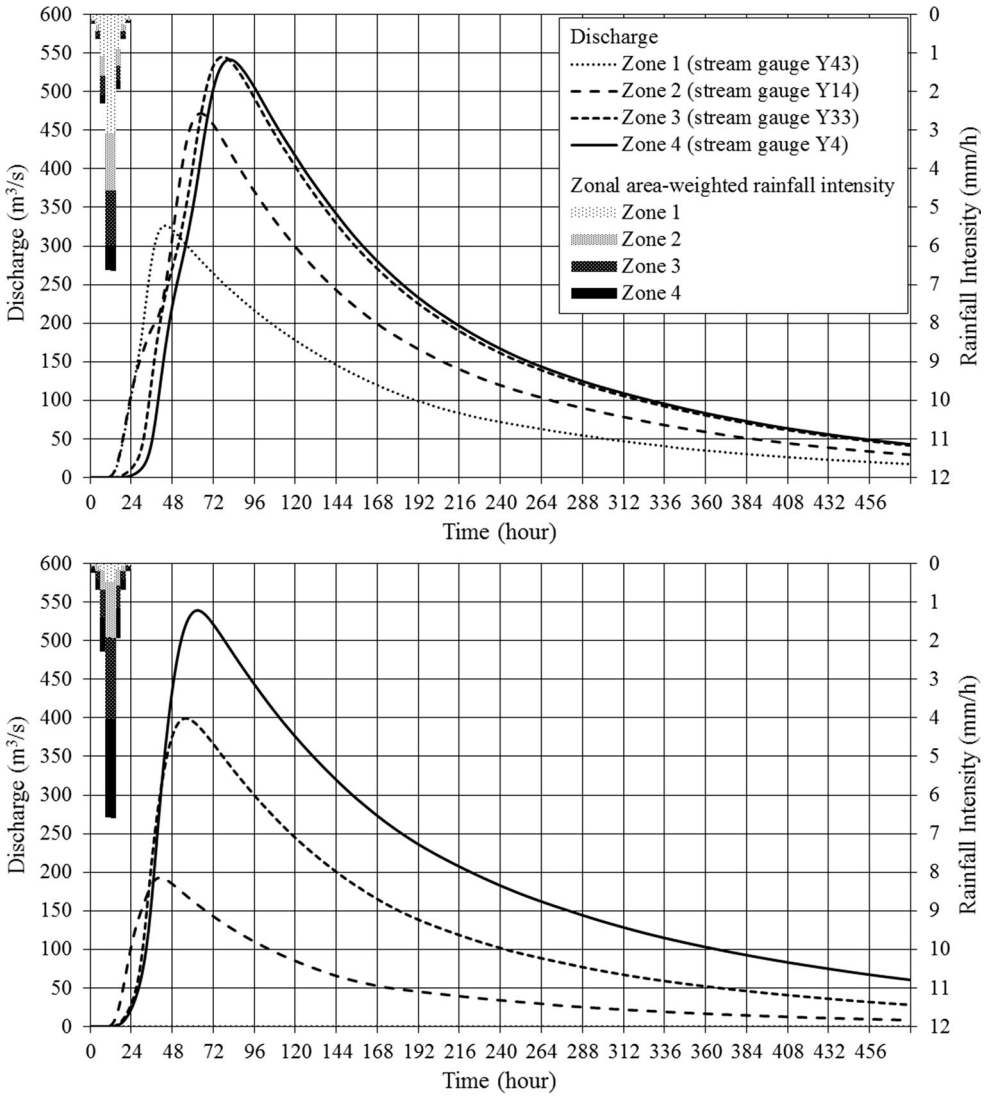

Fig. 9 Discharge from the sample of 24-h rainfalls with a 2-y return period that concentrated over the mountainous region (upper) and one sample of those over the plain area (lower)

are shown in Figs. 9 and 10 for the samples of 2-y and 10-y rainfalls, respectively.

From Table 5, when the amount of rainfall was small, the flood peak appeared to respond to the soil percolation rate and the surface storage rather than the steepness. The responses to these two characteristics are apparent when the rainfall was concentrated over the mountainous region. The flood peak responded to the rainfall in zones 1 and 2 rather than that in zones 3 and 4 because zones 3 and 4 had high surface water storage capabilities to retain the rainwater. Conversely, Table 6 shows that when the amount of rainfall was large, the flood peak appeared to respond to the steepness rather than the soil percolation rate and surface storage. This response to the steepness was apparent when the rainfall was concentrated over the plain area. The flood peak responds to the rainfall in zones 1 and 2 because these zones are steep, which causes the rainwater to be quickly drained to the stream. However, with both small and large rainfalls, the channel roughness had only a very small influence on the flood peaks.

4.3.2 Long-duration rainfall

The flood peak from a long-duration rainfall appeared to be mainly affected by the soil percolation rate at the rainfall location, because the long-duration rainfalls had lower intensities than the short-duration rainfalls. Apart from the soil percolation rate, there were effects of the surface storage and terrain steepness that depended on the rainfall magnitude, similar to the results of short-duration rainfall (Sect. 4.3.1). Tables 7 and 8 show the flood peaks from the 2-y and 10-y simulations, respectively, for samples 48-h rainfalls with each parameter adjusted to be uniform. The rainfall hyetographs and discharges at the outlets of the zones 1–4 for the usual case (no adjustment of parameter) are shown in Figs. 11 and 12 for the samples of 2- and 10-y

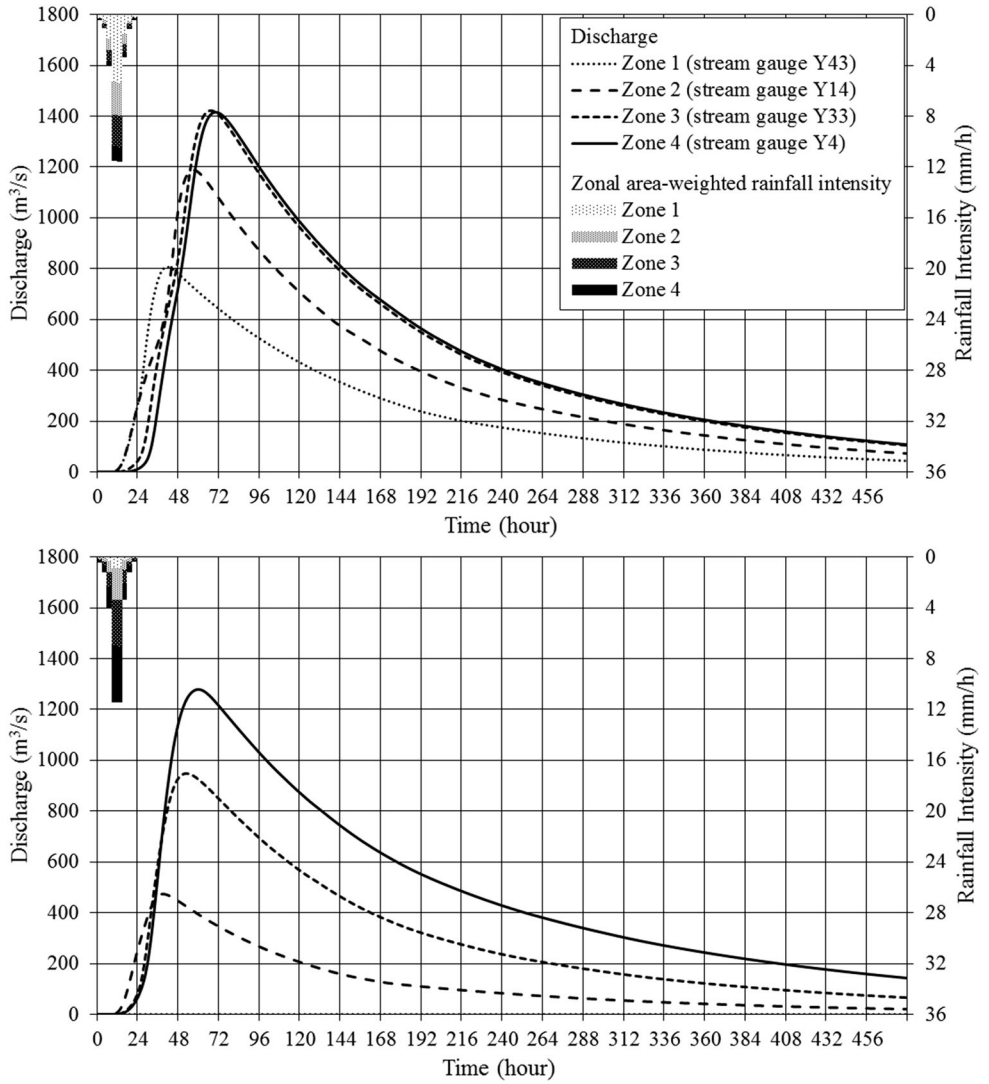

Fig. 10 Discharge from the sample of 24-h rainfalls with a 10-y return period that concentrated over the mountainous region (upper) and one sample of those over the plain area (lower)

Table 7 Peak discharge (m^3/s) from one sample of 48-h rainfalls with a 2-y return period that concentrated over the mountainous region and one sample of those over the plain area, when the basin coefficient, surface storage, Channel Manning's *n* and percolation rate were adjusted to be uniform

Adjustment detail	Concentrated over mountains		Concentrated over plains	
	Peak discharge	Difference[a]	Peak discharge	Difference[a]
Basin coefficient is 2.9	575.0	236.9	885.6	398.2
Basin coefficient is 5.8	338.1		478.4	
Surface storage is 0 mm	721.3	551.7	779.4	371.3
Surface storage is 30 mm	169.6		408.1	
Channel Manning's *n* is 0.047	490.1	80.4	524.8	35.4
Channel Manning's *n* is 0.019	570.5		560.2	
Percolation rate is 2.95 mm/h	365.4	792.5	210.1	762.7
Percolation rate is 0.45 mm/h	1157.9		972.9	
No adjustment	517.9	–	560.2	–

[a]Difference in the peak discharges between when parameter values at the mountainous region and plain area were used

Table 8 Peak discharge (m^3/s) from one sample of 48-h rainfalls with a 10-y return period that concentrated over the mountainous region and one sample of those over the plain area, when the basin coefficient, surface storage, Channel Manning's n and percolation rate were adjusted to be uniform

Adjustment detail	Concentrated over mountains		Concentrated over plains	
	Peak discharge	Difference[a]	Peak discharge	Difference[a]
Basin coefficient is 2.9	1870.9	814.3	2201.2	992.9
Basin coefficient is 5.8	1056.6		1208.4	
Surface storage is 0 mm	1818.6	652.0	1664.6	425.7
Surface storage is 30 mm	1166.6		1238.8	
Channel Manning's n is 0.047	1502.6	204.3	1388.5	135.0
Channel Manning's n is 0.019	1706.9		1523.5	
Percolation rate is 2.95 mm/h	1274.7	1182.5	982.6	1137.0
Percolation rate is 0.45 mm/h	2457.2		2119.6	
No adjustment	1608.8	–	1451.3	–

[a]Difference in the peak discharges between when parameter values at the mountainous region and plain area were used

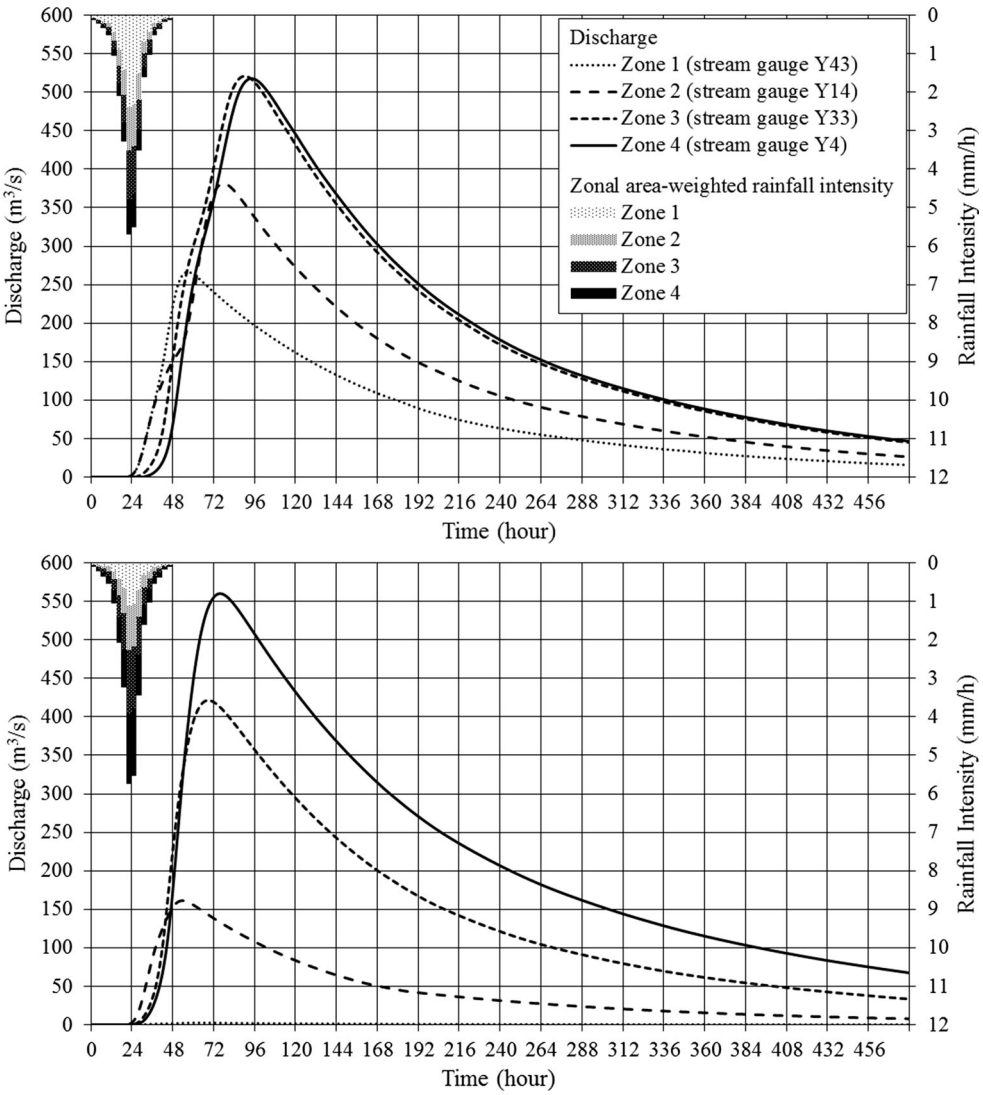

Fig. 11 Discharge from the sample of 48-h rainfalls with a 2-y return period that concentrated over the mountainous region (upper) and one sample of those over the plain area (lower)

rainfalls, respectively. It can be seen than the flood peak responded most strongly to the soil percolation rate at the rainfall location, followed by the surface water storage if the amount of rainfall was small and by the terrain steepness if the amount of rainfall was large. For the 72-h rainfall, a stronger influence of the soil percolation rate was

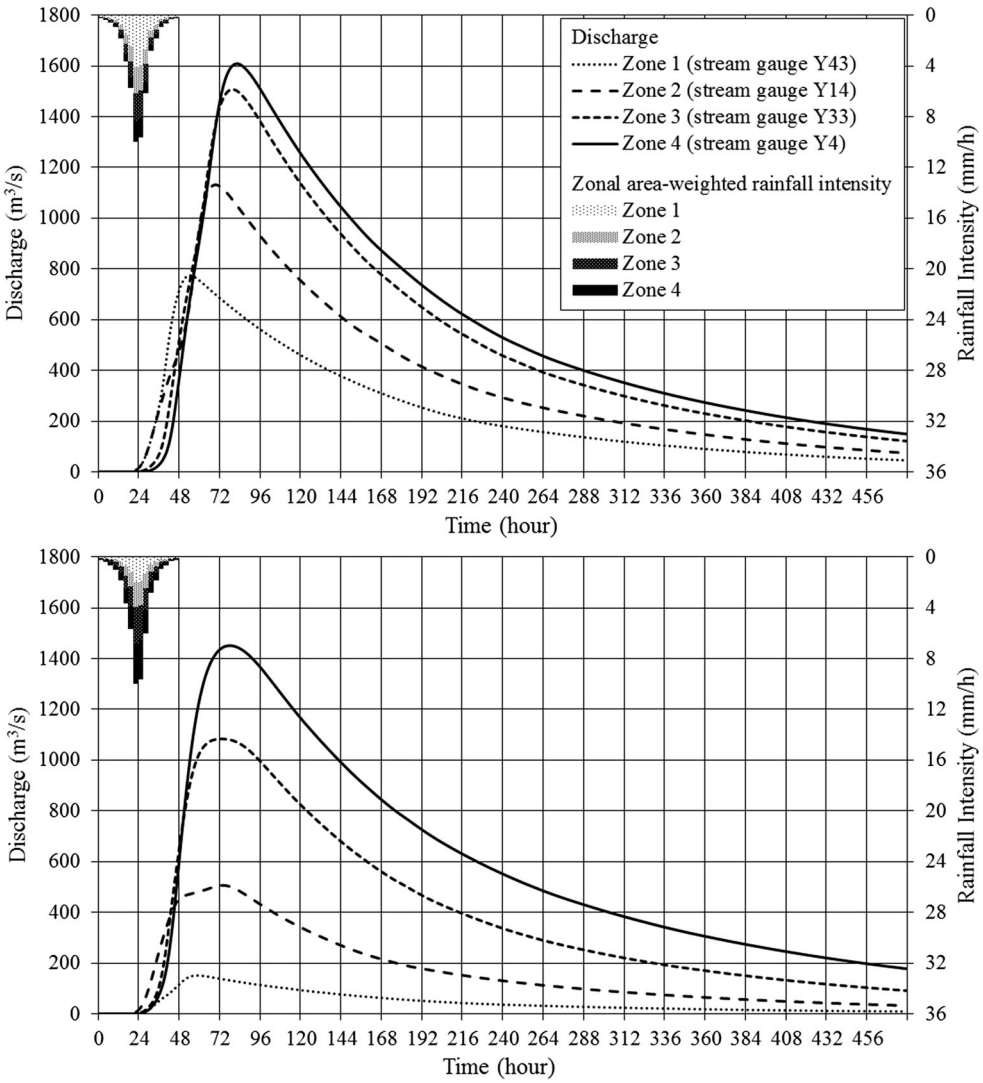

Fig. 12 Discharge from the sample of 48-h rainfalls with a 10-y return period that concentrated over the mountainous region (upper) and one sample of those over the plain area (lower)

expected because of the lower rainfall intensity than that in the 48-h rainfall.

Both zones 1 and 2 had a high soil percolation rate, but zone 1 had a lower rainfall magnitude than zone 2. In zone 1, the low rainfall intensity caused the influence of the percolation to be strong; therefore, most of the rainwater was lost to percolation. In zone 2, a higher rainfall intensity reduced the influence of the percolation. Thus, the correlation between the flood peak and rainfall was weak in zone 1 and strong in zone 2. Figure 13 shows the average of the peak excess rainfall intensity in each zone. Zone 1 had a lower peak excess rainfall intensity than zone 2, and the correlation between the flood peak and rainfall in zone 1 (Fig. 8) varied with the peak excess rainfall intensity, while that in zone 2 was always strong.

Compared to zone 3, zone 4 had a very long centroid distance (Table 1), which resulted in a very long standard lag time, t_p in Eq. (1); therefore, the flood peak from the rainfall in zone 4 was low. The standard lag time was 51 h for zone 4 but at most 32 h for the other zones. Thus, the correlation between the flood peak and the rainfall in zone 4 was always weak while that in zone 3 was always strong. This finding notes that the distance between the rainfall location and the main stream had a strong effect on the peak discharge, and so the presence of the main river in the model is necessary for the simulation of the flood peak from rainfall.

5 Conclusions

Although previous studies have reported the response of flood peaks to the spatial distribution of rainfall in large and nonuniform basins, the importance of each characteristic is still poorly understood. Thus, this study aimed to determine which characteristics are important for the response of the flood peak. The Yom River basin was chosen for this study because it has clearly different

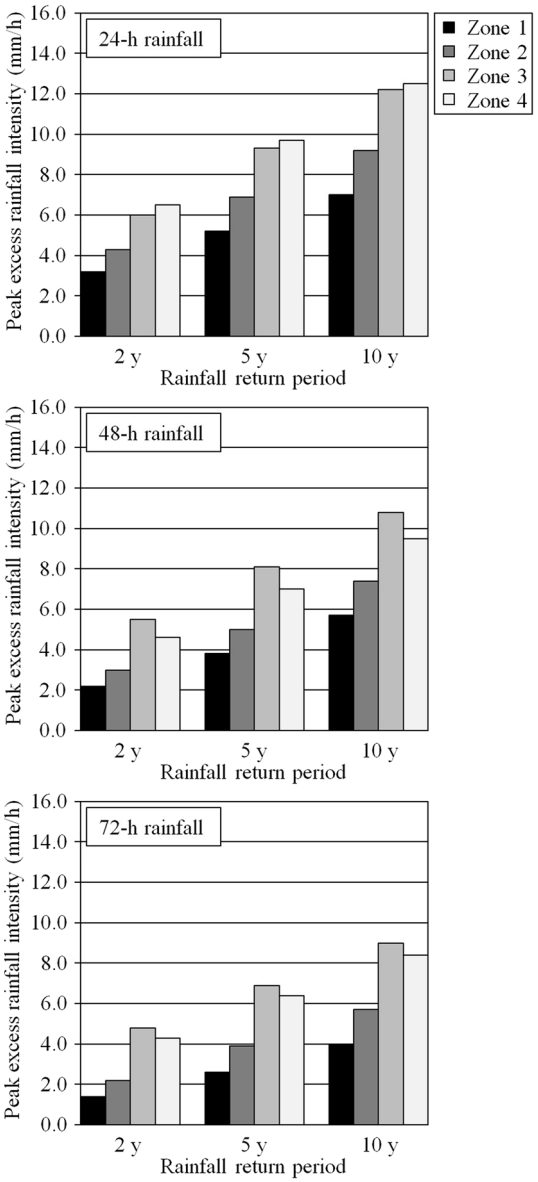

Fig. 13 Average peak excess rainfall intensity in each zone from the simulated rainfalls given a fixed rainfall amount for each return period and duration

characteristics between the upstream forested mountainous region with a small surface water storage and the downstream agricultural plain area with a large surface water storage. Moreover, since there are no large-scale control structures, the flow in this basin is nearly natural. The study area contains the city of Sukhothai, which is well known for being inundated by floods.

Floods in the Sukhothai area were simulated from rainfalls with various spatial distributions using the HEC-HMS and HEC-RAS models. The area which contributed the water to the Sukhothai city was divided into 8 subareas for routing the rainfall to the main stream, the Yom River, and the rainfalls were spatially distributed into four zones. Zones 1 and 2 represented the mountainous region with a high terrain steepness, high soil percolation rate and small surface water storage. Zone 3 was a plain area with a low steepness, low soil percolation rate and large surface water storage, while zone 4 was similar to zone 3 but was farther from the main stream. For each of 2-, 5- and 10-y rainfalls with 24-, 48- and 72-h durations, 1000 rainfall simulations with various spatial distributions were performed. The rainfall amounts in each of these four zones were spatially randomized according to the observed means, standard deviations and spatial correlations from a Monte Carlo analysis and Cholesky randomization. The rainfall tended to concentrate over the downstream part rather than the upstream part of the study area, and the 48- and 72-h rainfalls tended to concentrate upstream more than the 24-h rainfalls.

The simulations revealed that the flood peaks in the city of Sukhothai from a 24-h (short-duration) rainfall were usually low but highly variable, while the flood peaks from the 48- and 72-h (long-duration) rainfalls were high and fairly uniform. The correlation between the flood peak and rainfall in each zone suggested that a short-duration rainfall produced a high flood peak if it was concentrated over the upstream area (zones 1 and 2), while a long-duration rainfall produced a high flood peak if it was concentrated over the joint area (zones 2 and 3). The flood peak from a 24-h rainfall was usually low because this rainfall period is shorter than the concentration time; furthermore, 24-h rainfalls were rarely concentrated over the upstream area. Conversely, the flood peaks from 48 to 72-h rainfalls were high because the rainfall duration was similar to the concentration time, and these rainfalls tended to concentrate over the joint area. Usually, a high flood peak is generated from a long-duration rainfall, but it is possible for short-duration rainfalls to produce an extremely high flood peak if they are concentrated over the upstream area.

The basin characteristics that affect the response of the flood peak to the spatial distribution of the rainfall varied and depended upon the rainfall duration and amount. For a short-duration event with a small amount of rainfall, the flood peak was influenced by the surface water storage of the rainfall location. For a short-duration event with a large amount of rainfall, the flood peak is influenced by the steepness of the rainfall location. For a long-duration rainfall, the flood peak was mainly influenced by the percolation rate; in addition, the surface storage and steepness can be influential depending on the rainfall amount, similar to the case of the short-duration rainfall. Apart from the surface storage, steepness and soil percolation rate, the

flood peak responded to the distance from the rainfall location to the stream for both the short- and long-duration rainfalls. Therefore, the presence of the stream, especially a large stream, in the model is necessary for the flood peak simulation from the rainfall. Nevertheless, the channel roughness did not seem to influence the flood peak.

It should be noted that the influence of basin characteristics can vary upon the area and the result of the study strongly depends on the model parameterization. Therefore, the parameters should be carefully determined and the model validation is required from upstream to downstream areas, not only at the target area. For our study, because of long and narrow basin shape with a main river following the length direction, the parameterization in 2 parts (upstream mountainous region and downstream plain area) can make the model valid. For the complicate case when the area is wide, has many river branches and has variety of characteristics, the parameterization may be required in many parts of the area until the model is valid.

Acknowledgements This work was supported by the Japanese Government Scholarship (Grant number 132082), the Ratchadapisek Sompoch Endowment Fund (2017) of Chulalongkorn University (Grant number 760003-CC), the Office of Higher Education Commission (OHEC), and the S&T Postgraduate Education and Research Development Office (PERDO). Furthermore, we are grateful for the reviews by Professor Dr. George Christakos, Editor-in-Chief of Journal of Stochastic and Environmental Research and Risk Assessment, and anonymous reviewers.

References

Brunner GW (2010) HEC-RAS, river analysis system hydraulic references manual (version 4.1). US Army Corps of Engineers, Davis, CA

Chotpantarat S, Boonkaewwan S (2018) Impacts of land-use changes on watershed discharge and water quality in a large intensive agricultural area in Thailand. Hydrol Sci J. https://doi.org/10.1080/02626667.2018.1506128

Chotpantarat S, Chanyotha S (2003) The effect of land use changes on floods in Phetchaburi River Basin. In: Proceedings of 41th Kasetsart university annual conference: engineering and architecture. Thai National AGRIS Centre, pp 367–376

Chotpantarat S, Chuangcham K, Konyai S et al (2013) Water potential and demand research for sustainable water resources management in Yom River basin using conjunction use application and for land use planning in the future. Chulalongkorn University, Bangkok **(in Thailand)**

Chow VT, Maidment DR, Mays LW (1988) Applied hydrology. McGraw-Hill, New York

Feldman AD (2000) Hydrologic modeling system HEC-HMS: technical reference manual. US Army Corps of Engineers, Davis, CA

Freeze RA (1980) A stochastic-conceptual analysis of rainfall-runoff processes on a hillslope. Water Resour Res 16(2):391–408

Golian S, Saghafian B, Maknoon R (2010) Derivation of probabilistic thresholds of spatially distributed rainfall for flood forecasting. Water Resour Manage 24(13):3547–3559

Golian S, Saghafian B, Elmi M, Maknoon R (2011) Probabilistic rainfall thresholds for flood forecasting: evaluating different methodologies for modelling rainfall spatial correlation (or dependence). Hydrol Process 25(13):2046–2055

Hamidi A, Farnham DJ, Khanbilvardi R (2018) Uncertainty analysis of urban sewer system using spatial simulation of radar rainfall fields: New York City case study. Stoch Environ Res Risk Assess. https://doi.org/10.1007/s00477-018-1563-8

Higham NJ (2002) Computing the nearest correlation matrix—a problem from finance. University of Manchester, Manchester

Hunukumbura PB, Tachikawa Y (2012) River discharge projection under climate change in the Chao Phraya River basin, Thailand, using the MRI-GCM3.1S dataset. J Meteorol Soc Jpn 90A:137–150

Klongvessa P, Chotpantarat S (2014) Flood mitigation due to extreme rainfall events in the inner Bangkok, Thailand. Nat Hazards 73(3):1957–1975

Klongvessa P, Lu M, Chotpantarat S (2017a) Variation of characteristics of consecutive rainfall days over northern Thailand. Theor Appl Climatol. https://doi.org/10.1007/s00704-017-2208-4

Klongvessa P, Lu M, Chotpantarat S (2017b) Variation of critical rainfall duration upon its magnitude in middle and lower Yom basin, Thailand. J Water Resour Hydraul Eng 6(3):34–42

Kotsuki S, Tanaka K (2013) Impacts of mid-rainy season rainfall on runoff into the Chao Phraya River, Thailand. J Disaster Res 8(3):397–405

Kreyszig E (1999) Advanced engineering mathematics, 8th edn. Wiley, Hoboken

Kure S, Tebakari T (2012) Hydrological impact of regional climate change in the Chao Phraya River Basin, Thailand. Hydrol Res Lett 6:53–58

Lee G, Tachikawa Y, Sayama T, Takara K (2009) Effect of spatial variability of rainfall on catchment responses in mesoscale mountainous area. Ann J Hydraul Eng 53:7–12

Martins ES, Stedinger JR (2000) Generalized maximum-likelihood generalized extreme-value quantile estimators for hydrologic data. Water Resour Res 36(3):737–744

Meng C, Zhou J, Dai M, Zhu S, Xue X, Ye L (2017) Variable infiltration capacity model with BGSA-based wavelet neural network. Stoch Environ Res Risk Assess 31(7):1871–1885

Nkiaka E, Nawaz NR, Lovett JC (2018) Effect of single and multi-site calibration techniques on hydrological model performance, parameter estimation and predictive uncertainty: a case study in the Logone catchment, Lake Chad basin. Stoch Environ Res Risk Assess 32(6):1665–1682

Ogden FL, Julien PY (1993) Runoff sensitivity to temporal and spatial rainfall variability at runoff plane and small basin scales. Water Resour Res 29(8):2589–2597

Saghafian B, Golian S, Elmi M, Akhtari R (2013) Monte Carlo analysis of the effect of spatial distribution of storms on prioritization of flood source areas. Nat Hazards 66(2):1059–1071

Saghafian B, Golian S, Ghasemi A (2014) Flood frequency analysis based on simulated peak discharges. Nat Hazards 71(1):403–417

Samadi S, Tufford DL, Carbone GJ (2018) Estimating hydrologic model uncertainty in the presence of complex residual error structures. Stoch Environ Res Risk Assess 32(5):1259–1281

Sayama T, Tatebe Y, Iwami Y, Tanaka S (2015) Hydrologic sensitivity of flood runoff and inundation: 2011 Thailand floods in the Chao Phraya River basin. Nat Hazards Earth Syst Sci 15(7):1617–1630

Sayama T, Tatebe Y, Tanaka S (2017) An emergency response-type rainfall-runoff-inundation simulation for 2011 Thailand floods. J Flood Risk Manag 10(1):65–78

Singh VP (1992) Elementary hydrology. Pearson College Division, Englewood Cliffs, NJ

Singh VP (1997) Effect of spatial and temporal variability in rainfall and watershed characteristics on stream flow hydrograph. Hydrol Process 11(12):1649–1669

Sriariyawat A, Pakoksung K, Sayama T, Tanaka S, Koontanakulvong S (2013) Approach to estimate the flood damage in Sukhothai Province using flood simulation. J Disaster Res 8(3):406–414

Tingsanchali T, Karim F (2010) Flood-hazard assessment and risk-based zoning of a tropical flood plain: case study of the Yom River, Thailand. Hydrol Sci J 55(2):145–161

Tramblay Y, Bouvier C, Ayral PA, Marchandise A (2011) Impact of rainfall spatial distribution on rainfall-runoff modelling efficiency and initial soil moisture conditions estimation. Nat Hazards Earth Syst Sci 11:157–170

Zoccatelli D, Borga M, Viglione A, Chirico GB, Blöschl G (2011) Spatial moments of catchment rainfall: rainfall spatial organisation, basin morphology, and flood response. Hydrol Earth Syst Sci 15:3767–3783